JOURNAL OF MECHANICAL ENGINEERING AND SCIENCES
ISSN: 2289-4659 e-ISSN: 2231-8380
VOLUME 18, ISSUE 3, 2024, 10140 - 10160
DOI: https://doi.org/10.15282/jmes.18.3.2024.4.0801

UNIVERSITI MALAYSIA PAHANG AL-SULTAN ABDULLAH

RESEARCH ARTICLE

Three-dimensional simulation of finite element ultrasonic welding of aluminum alloy AA-6061

H. T. M. Nu, D. L. C. Ky, L. T. Truyen*

Department of Mechanical Engineering, Ho Chi Minh University of Industry and Trade, 70000, HCM City, Vietnam
Phone: +084 907570891

ABSTRACT - Ultrasonic metal welding is often used as a rapid and effective technique for joining sheet metals without causing them to melt. Precise management of the welding process parameters is crucial for achieving excellent joint quality. However, modeling the behavior of the weld material and the welding process is still very challenging. This study aimed to create 3D finite element models that accurately simulate the ultrasonic metal welding process. The proposed material model integrates frictional heat and ultrasonic softening, as well as the cyclic plasticity model. A friction law incorporating a variable friction coefficient is examined to investigate surface impacts. This coefficient is influenced by contact pressure, slippage, temperature, and the number of cycles. The findings of this study demonstrate that the oscillation frequency significantly influences both the temperature fluctuation and the extent of the heat-affected zone. Increased frequencies lead to accelerated temperature fluctuations and expanded heat-affected. Furthermore, ultrasonic welding combined with preheating led to a much wider heat-affected zone than ultrasonic welding without heating. The minimum preheating temperature required for ultrasonic welding of aluminum is 150 °C. This model can predict the relative displacement between welded plates. Assessing the oscillations that arise during the ultrasonic welding process is beneficial in selecting suitable welding settings to prevent excessive heating. This aids engineers in choosing appropriate welding parameters to avoid excessive heat generation during ultrasonic welding, hence limiting the reduction in tensile strength of the weld. Consequently, it can decrease the expense of the experimental methodology.

ARTICLE HISTORY
Received : 18th Mar. 2024
Revised : 19th June 2024
Accepted : 20th Aug. 2024
Published : 30th Sept. 2024

KEYWORDS
Aluminium
Finite element model
Li-ion battery
Ultrasonic welding
Modelling

1. INTRODUCTION

The growing demand for eco-friendly fuels is fueling a substantial shift in the hybrid and electric automobile industry [1]. These vehicles obtain the required capacity by using lithium-ion battery packs. Battery packs sometimes consist of several individual battery cells, and aluminum is often used for connections in battery manufacturing owing to its remarkable electrical and thermal conductivities. Conventional fusion welding methods to connect thin materials present challenges because of the frequent presence of fragile intermetallic compounds at the junction interface. Consequently, the manufactured joint lost its strength. Solid-state welding techniques, such as ultrasonic welding, minimize heat generation during the welding process and enable the formation of connections at temperatures below the material's melting point. Consequently, the probability of intermetallic compound formation was significantly reduced. Therefore, ultrasonic welding techniques are widely used in the automotive industry to connect battery terminals. Ultrasonic welding (USW) is a technique that uses both constant pressure and high-frequency vibrations simultaneously to join metal sheets, creating a bond without melting the components. This method produces welds without melting and applies to welding comparable or dissimilar materials. Moreover, they offer the benefits of low energy use and do not require additional chemicals [2]. The microstructure quality at the weld interface in USW depends on the level of heat production and plastic deformation. Choosing the correct process parameters significantly affects the quality. Previous studies have shown that the amalgamation of frictional heating, intense plastic deformation, and localized melting may create solid-state bonds between different metals. Frictional heat and heat from plastic deformation are often considered the main factors contributing to weld formation. To fully comprehend the welding process, the temperature distribution, heat production, and level of plastic deformation must be analyzed since fluctuations in input parameters affect the energy transferred to the weld spot.

Experimental methods have recently been widely used to study ultrasonic metal welding (UMW) processing principles. Tsujino et al. [3] studied using upper and lower welding electrodes to connect an aluminum alloy plate and stainless steel. The technology reportedly functions with a power output of around 50 kilowatts to join together panels that are 6 mm thick. Watanable et al. [4] investigated the ultrasonic welding technique of mild steel plate with an Al-Mg plate in their investigation. This study revealed that the tensile strength of the weld decreased as the welding time and pressure increased. Kong et al. [5-7] conducted ultrasonic welding of two distinct aluminum alloys, AA 6061 and AA 3003. This research demonstrates that the hardness close to the weld contact is greater than that at a distance from the

*CORRESPONDING AUTHOR | L. T. Truyen | ✉ truyenlt@hufi.edu.vn

weld interface. The variation in the hardness values is attributed to two factors: the frictional influence on the contact surface of the weld and the acoustic softening that occurs in the material during the welding process. The research conducted in [8] aimed to investigate the relationship between the duration of the welding process and the interface temperature and joint strength of Al-Cu welds. It has been shown that it is important to use higher vibration amplitudes and shorter welding durations to achieve sufficient strength. Regarding AA6061 aluminum, the research done by Yang et al. [9] showed that the duration of the welding process directly affects the welds' shear strength. As the duration of the welding process increased, the shear strength increased until it reached a certain threshold, beyond which it began to decrease. Cheng and Li [10] investigated the process of ultrasonic metal welding using a microsensor array positioned between a copper alloy and nickel substrate. They specifically focused on analyzing heat production and temperature changes throughout welding. Balz et al. [11] implemented sensor signals to oversee the ultrasonic metal-welding manufacturing of lithium-ion batteries. These signals are strongly correlated with the quality of joints produced under various production settings. The findings of this investigation demonstrate that using low welding temperatures and inducing plastic deformation results in ultrasonic welds of superior quality. In contrast, high temperatures and significant plastic deformation result in welds of poor quality. Zhao et al. [12] experimented to assess the impact of welding energy on Al-Cu ultrasonic welds at different levels of ultrasonic energy. When the welding energy decreased, only a few welds were visible at joint contact. Splicing fails at a relatively modest demand owing to the connection loss. Elangovan et al. [13] found that the duration of ultrasonic welding of copper has the most significant influence on the strength of the joint, with the welding amplitude and pressure being of lesser importance.

Several researchers are interested in conducting computer simulation studies on ultrasonic welding, in addition to experimental investigations, to address the limitations of the experimental studies. Process modeling and simulation play a vital role in designing and enhancing the UMW process by establishing a connection between the process parameters and the features and performance of the weld. Models may offer valuable insights into the design of a knurl shape by demonstrating how it affects the contact and friction behavior while forming a joint. A connection was discovered between the weld's process parameters, features, and efficiency. Nevertheless, major obstacles impede the development of computationally effective models for the UMW process. The first is to simulate the significant interactions between the mechanical, thermal, and metallurgical domains. Materials experience nonlinear hardening and mostly friction-induced thermal softening during the UMW process under 20 kHz cyclic loading, impacting heat production. When subjected to ultrasonic loading, materials often experience substantial acoustic softening, resulting in decreased flow stress during operation. Acoustic softening is a natural phenomenon resulting in dislocation annihilation and subgrain growth. Siddiq and Ghassemieh [14] conducted a thermomechanical analysis of the ultrasonic welding of aluminum alloys. The suggested cyclic plastic model, including the thermal and acoustic relaxation factors, considers the influence of both volumetric and surface effects. Elangovan [13] experimented using copper plates with different thicknesses. The findings obtained from the experiment were further verified by finite element analysis (FEA). In contrast to the usual parabolic pattern in temperature measurements, the projected temperature has a linear correlation with time. Jedrasiak et al. [15] created a mathematical model using finite element analysis to simulate the ultrasonic welding process. The model specifically focused on welding aluminum 6111 with magnesium AZ31 and low-carbon steel DC04. The second difficulty involves modeling the dynamic weld production process and capturing the detailed material reaction while considering the boundaries of the 3D geometry of the UMW welder tools and high-frequency vibration loading. Lee et al. [16] used 2D modeling to perform finite element simulations of the UMW pin tab. An investigation was conducted on the influence of horn geometry on the distribution of plastic deformation in the specimen. Chen and Zhang [17] conducted a numerical study of ultrasonic welding to ascertain the impact of horns on samples. Their study demonstrated stress, plastic deformation, and compression-direction deformation due to vibration. Li et al. [18] created a 3D thermomechanical finite element model for different materials (aluminum and copper) in a two-layer lap-welding setup. They included material softening and high convection boundary conditions in their simulation but did not explicitly describe the ultrasonic vibration of the horn. Presently, the primary emphasis of simulations is directed toward investigating the impact of the horn shape on the plastic deformation and stress of the weld [16 - 18]. There is a lack of research on the movement of welded plates, which might be used to forecast overheating in ultrasonic welding.

To remain competitive with other battery production processes, such as laser welding and resistance welding, and to fully exploit the benefits of ultrasonic metal welding, it is essential to have in-depth knowledge of the process mechanics and its effects. Most previous research has been concentrated on laboratory studies that examine the impact of ultrasonic welding settings. The process parameters are typically established through an iterative process of experimentation and refinement. Currently, there is a limited theoretical understanding and explanation of the factors that contribute to the success of the process in certain situations, as well as the reasons for its failure in other cases. Moreover, there has been a lack of sufficient study on the preheating of welded components before the ultrasonic welding procedure. Furthermore, we may examine the relative displacement of the joined plates by employing simulation data, thereby eliminating the need for expensive measuring devices commonly used in experimental processes. Analyzing the relative motion of plates might help predict when overheating may happen in ultrasonic welding, leading to a decrease in the weld's tensile strength. However, the existing process models described in the literature have not yet addressed the challenge of accurately calculating the movement between welded plates.

This research aims to analyze the vibration characteristics of the UMW process using numerical simulation approaches, considering different production settings. This study utilizes Abaqus/CAE 2017 software to construct a

complete 3D model incorporating a thermomechanical multiphysics simulation model. The model encompasses oscillatory motion, friction, and heat generation during ultrasonic welding between two aluminum plates measuring 0.08 mm thick. This study employed friction models that consider the dependence on temperature and pressure rather than assuming a constant friction coefficient. The finite model in this study also incorporates a kinematic friction model that considers the influence of surface effects in the ultrasonic welding process and a material model based on cyclic plasticity theory to account for phenomena occurring inside the bulk material. This study examines the relative motion of aluminum panels using a 3D model. Analyzing the observed relative movements can provide insight into the predicted condition of the ultrasonic welded joint. In particular, the welding method with local pre-heating increases the heat-affected area and creates a uniform heat distribution, thereby increasing the reliability of the ultrasonic weld. Ultimately, the simulation findings obtained from this work may be used to identify the most appropriate welding process settings, hence reducing the need for trial and error testing.

2. MATERIALS AND METHODS

Ultrasonic welding forms a connection by utilizing the ultrasonic vibration energy on the welding material. This procedure involves the application of a force in the direction perpendicular to the surface of the workpiece, resulting in compressive loading. In addition, cyclic loading was applied in the tangential direction. The outcome of these two motions is heat production due to friction and an elevation in the temperature at the point of contact. Therefore, this procedure is regarded as a linked thermomechanical issue. The concept of ultrasonic welding is illustrated in Figure 1. The ultrasonic welding procedure comprised two main stages: clamping and vibration. A clamping force was applied perpendicular to the front surface of the knurl. Knurl can move vertically, whereas the anvil remains stationary in every direction. The vibrations induce friction in the materials, increasing the contact surface temperature. The rapid heat generation due to friction creates the necessary circumstances for the materials to adhere to each other. This paper presents a simulation analysis of ultrasonic welding of aluminum alloys (AA) 6060/6061. This aluminum alloy is frequently utilized because of its thermal and mechanical qualities, which make it highly adaptable. AA 6060/6061 is widely used in several industries, including aerospace, marine, automotive, and electrical/electronic, because of its excellent strength, surface polish, weldability, and workability.

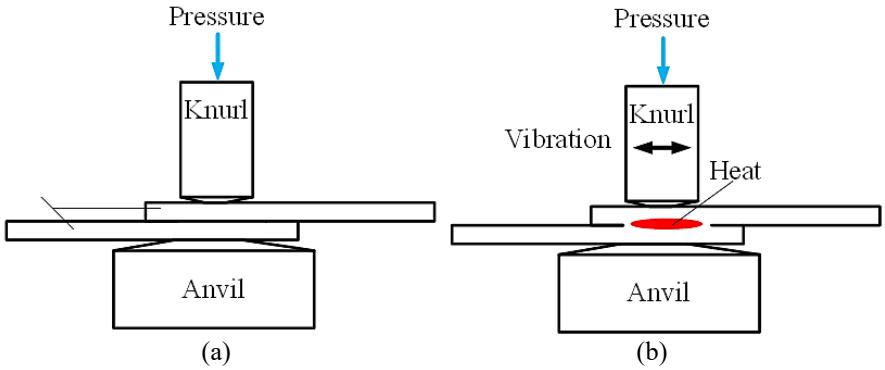

Figure 1. Ultrasonic welding process: (a) clamping and (b) vibration

This study examined the USW process using a FEA model. Unlike the modeling strategy used in conventional fusion welding techniques, such as arc welding or laser welding, heat transport analysis must be conducted concurrently. Concurrent with the mechanical analysis, ultrasonic welding produces heat due to frictional action at different interfaces and the spread of plastic deformation in the sheet material. Hence, it is crucial to consider the ultrasonic welding process as a mechanical-thermal issue. The model must explicitly include vibrations of the knurl, deformation of the plate, and heat transmission. This study used a 3D model with two analytical steps: clamping and knurl vibration. A temperature forecasting model was constructed that incorporates fluctuations in temperature and pressure, considering the effects of friction. Frictional heat is generated when mechanical friction occurs at the sliding contact because of localized shear stresses.

2.1 Mechanical Model

2.1.1 Isothermal cyclic plasticity model

The mechanical aspects of ultrasonic welding include repetitive sideways movement and pressure used to hold the workpieces together. Chaboche [19] presented a brief overview of a constitutive model suitable for evaluating the malleability of metals under repeated loads. The underlying assumption is that the total rate of deformation, $\dot{\boldsymbol{\varepsilon}}$ can be decomposed into its individual components:

$$\dot{\varepsilon} = \dot{\varepsilon}^{el} + \dot{\epsilon}^{pl} \tag{1}$$

The terms $\dot{\varepsilon}^{el}$ and $\dot{\varepsilon}^{pl}$ represent the elastic and plastic components of the overall strain rate. The following model may represent the elastic behavior at every given stage of the simulation:

$$\sigma = D^{el} : \varepsilon \tag{2}$$

The 4th-order elasticity tensor is denoted as D^{el}, whereas the 2nd-order stress and strain tensors are represented by σ and ε, respectively. The operator ":" in Eq. (2) denotes the scalar product, which may be expressed in the Einstein notation as a: $b = a_{\alpha\beta}b_{\beta\alpha}$. Here, a and b are tensors, while α and β are indices representing components of both tensors. The yield function, often known as the criteria, is expressed as:

$$F = |\sigma - \propto| - (\sigma_0 - R) = 0 \tag{3}$$

The term α represents the reverse stress tensor, σ_0 represents the initial yield stress, and R represents the term associated with isotropic strain hardening. The plastic behavior during deformation is provided.

$$d\varepsilon^{pl} = d\lambda \frac{\partial F}{\partial \sigma} \tag{4}$$

where $d\lambda$ is the plasticity multiplier that satisfies the following Kuhn-Tucker consistency condition:

$$F \leq 0;\ d\lambda \geq 0, d\lambda . F \cong 0 \tag{5}$$

Isotropic hardening, R quantifies the expansion of the yield surface and is theoretically represented as an exponential function of the accumulated plastic strain. Isotropic hardening is affected by past plastic strain [20-23]:

$$R = Q\left(1 - e^{-b\underline{\varepsilon}^{pl}}\right) \tag{6}$$

where Q and b are material parameters in which Q is the maximum change in the size of the yield surface, and b is the rate at which the size of the yield surface changes with the plastic strain and $\underline{\varepsilon}^{pl}$.

The nonlinear isotropic/kinematic hardening rule mentioned above necessitates the determination of parameters (Q, b, C) based on cyclic stress-strain data, thermal softening data, and acoustic (ultrasonic) softening data. The isothermal material parameters (Q, b, C, γ) are listed in Table 1 [14].

Table 1. Identified nonlinear isotropic/kinematic hardening parameter

Q (MPa)	b	C (GPa)	γ
100	20	15	60

2.1.2 Cyclic plasticity model with thermal softening

Several metals that undergo aging have a significant influence on the temperature path history [25]. The current analysis adopted the thermomechanical term from the hardening model proposed by Johnson and Cook [26]. The incorporation of this thermomechanical coupling term is simple. The revised nonlinear isotropic hardening law is expressed as:

$$R_\infty = Q\left(1 - e^{-p\underline{\varepsilon}^{pl}}\right)(1 - T_\infty^m) \tag{7}$$

The material parameter is denoted as m, whereas the non-dimensional temperature is represented by T_∞ as

$$T_\infty = \frac{(T - T_1)}{(T_m - T_1)} \tag{8}$$

T_1 represents the transition temperature below which the yield stress does not vary, whereas T_m corresponds to the temperature at which melting occurs.

2.1.3 Cyclic plasticity model with thermal and ultrasonic softening

Acoustic softening, also known as ultrasonic softening, refers to a reduction in the plastic limit of a material when subjected to strong ultrasonic vibrations. Exploration of acoustic softening has been ongoing for several decades. A phenomenological factor that caused a decrease in hardness was added to the equations for isotropic and kinematic hardening. This term depends on the amount of ultrasonic energy per unit of time. The temperature-dependent initial yield

of aluminum alloy Al 6061 was determined using an experimental fit utilizing data from experiments [14, 26]. The experimental temperature-dependent initial yielding was best represented by the fit given in Figure 2 [14, 27]. Figure 3 shows the relationship between the initial yield stress obtained via experimentation and simulation and the ultrasonic energy density per unit of time. These figures demonstrate a high level of agreement.

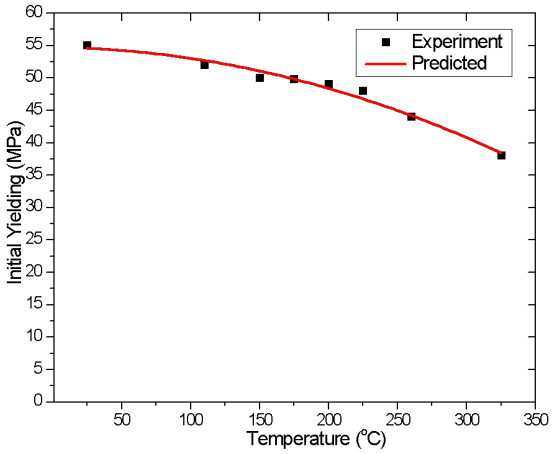

Figure 2. Temperature-dependent initial yielding [27]

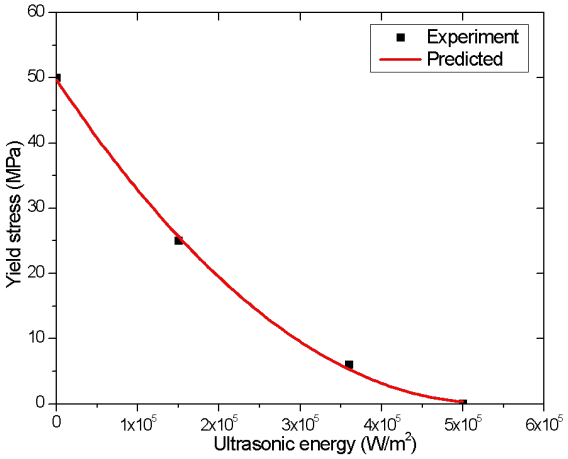

Figure 3. Influence of the rate of ultrasonic energy application on the onset of yielding [27]

2.2 Thermal Model

This study considered materials' thermal and mechanical properties that change with temperature. The empirical data on the correlation between the thermal coefficients and temperature were converted into equations to improve the accuracy of the simulation results. The thermal concerns of the workpiece in ultrasonic welding require meticulous attention because of the significant heat generated from the friction between the workpieces. To address this issue, it is necessary to solve the conduction and mechanical constitutive equations. The conduction equation is as follows:

$$\rho c(T)\frac{\partial T}{\partial t} = -\vec{\nabla}.\left(-k(T)\vec{\nabla}T\right) + S \tag{9}$$

The symbols ρ, T, and (T) denote the material's density, specific heat, and thermal conductivity, respectively. In this inquiry, the quantity S in Eq. (9) represents the volumetric heat production; however, it is not considered.

The main source of heat generation in the ultrasonic welding process is the dissipation of frictional heat caused by the rubbing of adjacent workpieces. Therefore, to analyze the thermal properties of the workpieces in this process, it is essential to use models that include both friction and heat dissipation resulting from friction. The Coulomb friction model was used in this study. The dissipation of heat due to friction, denoted as q^{fr}, may be determined when there is relative motion between the two workpieces:

$$q^{fr} = \eta.\mu.\dot{s} \tag{10}$$

The variable η denotes the fraction of heat dissipation caused by friction, ranging from 0 to 1. The symbol $\dot{s}$ depicts the velocity change rate in the sliding motion, while μ is used to express the friction coefficient. The parameter η is not explicitly known but may be implicitly deduced from experimental data. The ultrasonic welding process requires the consideration of a thermal factor called gap conductance, which generates a temperature discontinuity between two workpieces in contact with each other. The word "gap conductance," represented by the symbol κ, is precisely defined as:

$$q^{g} = \kappa.\Delta T \tag{11}$$

The variable q^{g} indicates the heat transfer between the two surfaces of the workpieces in contact, whereas ΔT represents the difference in temperature between these two surfaces. The gap conductance, as inferred from their experimental findings, relates to a particular contact configuration and surface irregularities [28]:

$$G = \frac{k_g}{\kappa.f} \tag{12}$$

The symbol k_g represents the heat conductivity of the gas present between the two workpieces. The effective gap distance, denoted by f, is governed by surface roughness and clamping pressure. Therefore, the gap conductance can be approximately calculated using this equation, assuming the effective gap distance and thermal conductivity of air. Their findings suggest that $G = 1$ when the gas pressure is at atmospheric levels.

2.3 Friction Model

The friction model is essential for generating heat during ultrasonic welding, particularly in the initial stage. The traditional Coulomb model determined the friction force acting on the contact surfaces [29]. The friction model presented in this study is based on the correlation between the coefficient of friction and many factors, including the number of cycles *N*, temperature *T*, and parameters *a* and *b*, which are contingent upon the magnitude of the slip and contact pressure, as presented in Eq. (13) [30].

$$\mu_0 = \mu_s + \mu_s(a.log\ log\ (N)\ + b) \tag{13}$$

The coefficient of friction positively correlates with the number of cycles, gradually increasing until it reaches a certain threshold, at which point it stabilizes and remains constant. The friction behavior was analyzed using a straightforward logarithmic correlation. The friction coefficients, denoted by *a* and *b*, are contingent on the slip amplitude and contact pressure. Conversely, μ_s represents the initial static coefficient of friction, and *N* signifies the number of cycles. The values of variables *a* and *b* were determined using different levels of contact pressure and displacement amplitudes [31]. Zhang et al. [29] examined temperature and friction coefficient correlations. Empirical evidence indicates that the coefficient of friction exhibits an upward trend with increasing temperature until it reaches a certain threshold, beyond which it decreases. The impact of temperature on this phenomenon was considered by including an additional fourth-degree polynomial as a function that varies with temperature. The modified coefficient is given by:

$$\mu = \mu_0.(p.T^4 + q.T^3 + r.T^2 + s.T + t) \tag{14}$$

The additional friction parameters *p*, *q*, *r*, *s*, *t* were identified using the experimental results as *p* =8.485E-10, *q* = -8.842E-7, *r* = 1.969E-4, *s* =9.762E-3, *t* = 1.12 [14]. The existing friction subroutine was enhanced by incorporating Eqs. (13) and (14), respectively. This was achieved by substituting the constant coefficient of friction with temperature-dependent, contact pressure-dependent, vibration-dependent, and cycle-dependent friction coefficients. Tables 2 and 3 provide information on aluminum and steel's thermal and mechanical properties, respectively.

Table 2. Thermal and mechanical properties of AA 6060/6061

Thermal Properties		Elastic Properties	
Thermal conductivity (W $m^{-1}K^{-1}$)	235	Young's modulus (GPa)	66.24
Thermal expansion coefficient ($^oC^{-1}$)	23×10^{-6}	Poisson's ratio	0.33
Specific heat (J $kg^{-1}K^{-1}$)	896	Yield stress (MPa)	50
Density (kg m^{-3})	2700		

Table 3. Thermal and mechanical properties of steel (for knurl and anvil)

Thermal Properties		Elastic Properties	
Thermal conductivity (W $m^{-1}K^{-1}$)	80	Young's modulus (GPa)	200
Thermal expansion coefficient ($^oC^{-1}$)	11×10^{-6}	Poisson's ratio	0.27
Specific heat (J $kg^{-1}K^{-1}$)	440		
Density (kg m^{-3})	7800		

2.4 Validation Method

To assess the reliability of the finite element model, this article compares the results obtained from welding process simulation with experimental studies published in recent years.

3. RESULTS AND DISCUSSION

An Abaqus/Explicit program was used to develop a 3D thermomechanical coupling model to study the thermomechanical coupling effect in ultrasonic welding. The suggested model can interact with the input parameters related to the temperature distributions, energy, and material displacement in the ultrasonic welding process. During ultrasonic welding, the horn tip may undergo perpendicular vibrations to the plates despite efforts to minimize these vibrations through the design of the horn tips. Furthermore, the texture of the sheet is rough. However, this finite element model assumes the sheets are perfectly flat and free from vibrations perpendicular to the horns' motion. Furthermore, the model considers the prescribed displacement boundary conditions, accounting for any undesired displacements resulting from the constraints of the physical mounting apparatus in real-life situations.

3.1 Model Geometry

Figure 4 illustrates a standard configuration for ultrasonic metal welding. The welding configuration has three primary elements: sheet metal, an anvil, and a knurl affixed to the ultrasonic welding unit. The knurl vibrates in a direction that is

perpendicular to the rolling welding direction. The knurl in this variant has dimensions of 10 mm × 10 mm × 12 mm, whereas the anvil has dimensions of 120 mm × 45 mm × 12 mm. Knurls and anvils both have flat surfaces. The aluminum sheets had a thickness of 0.08 mm with a specified size of 120 mm × 45 mm.

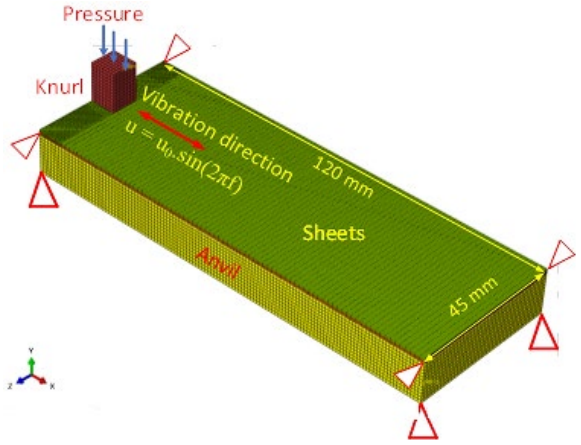

Figure 4. Finite element model

3.2 Mesh

In this welding process simulation, we treated the knurl and anvil as rigid bodies and meshed them with a size of 0.4 mm, resulting in 768 and 67500 elements, respectively. We divided the workpiece's upper and lower parts into two partitions: a refinement region and a coarse region. We meshed the refinement region, measuring 8 × 0.8 × 45 mm, with 4600 elements, using a mesh size of 0.4 mm in the U_X and U_Z directions and 0.4 mm in the U_Y direction. Greater refinement results in more elements and increased accuracy, leading to longer computation times. We also meshed the coarse region, measuring 117 × 0.8 × 45 mm, with 18860 elements, using a mesh size of 0.5 mm in the U_X and U_Z directions and the same value in the U_Y direction as the refinement region. The Abaqus 8-node brick element, namely the C3D8RT element with reduced integration and hourglass control, was utilized. This element is suitable for coupled thermal-mechanical analyses, where temperature distribution and structural deformations need to be considered. The Arbitrary Lagrangian-Eulerian (ALE) adaptive mesh feature of Abaqus is utilized for sheets and the interconnect to mitigate any numerical challenges arising from significant mesh distortion. The Arbitrary Eulerian-Lagrangian re-meshing approach aims to enhance the deformation zone in simulations, hence preventing divergence caused by localized excessive deformation.

3.3 Step

The Abaqus/Explicit solver was chosen for the high-fidelity model of the highly dynamic thermomechanically coupled UMW process. The model faithfully simulates the ultrasonic welding process, which consists of two stages, clamping and sonotrode vibration, and correctly represents real-world circumstances. The initial stage involves applying the displacement of the horn to replicate the trigger force, which then applies compressive pressure to clamp the two workpieces together. The second stage begins with the vibration of the horn.

3.4 Boundary Conditions

The boundary and loading settings for the clamping and welding processes simulations are shown in Figure 4. During the clamping stage, the movement of the edge nodes of the sheets was restricted in the ultrasonic welding direction. Specifically, the displacements in the U_X and U_Z directions were confined to zero, whereas that in the U_Y direction was not restricted. The knurl displacement was restricted to the same direction, and for the rotational displacement on the XY plane, the θ_z value remained constant at 0. The movement of the anvil is completely restricted, the same as during the real experiments. In practice, these boundary conditions are achieved using specialized fixtures.

The sonotrode tip is subjected to pressure and uniformly distributed throughout its top surface. Practically, this pressure corresponds to the clamping pressure determined by the clamping load of the ultrasonic welding machine and the dimensions of the actual tool employed. The clamping force was represented by a time-dependent function that progressively increased from zero to the required magnitude. The transition took place within 2.5 milliseconds using Abaqus's smooth step amplitude. The simulation used clamping pressures of 50 MPa, 75 MPa, and 100 MPa. The clamping force was selected to prevent excessive plastic deformation owing to the constraints of the linked kinematic isotropic hardening model. When vibration has begun, the tip oscillates horizontally in the U_X-direction. The tip is limited to moving in horizontal and vertical dimensions and is prevented from rotating. All the workpieces were subjected to a gravitational acceleration of 9.81 ms^{-2}. The entire model was subjected to a specified room temperature of 24 ºC as the beginning temperature.

The clamping process was initially simulated under predetermined parameters. The results obtained from the clamping step were subsequently employed as the beginning parameters for the welding phase. During the initial stage of the welding phase simulation, variations were noted in the boundary and loading conditions. The displacement limits of the sheet nodes were removed. The knurl displacement constraint in the U_X-direction is substituted with a cyclic displacement condition, expressed as $u(t) = u_0.sin(2\pi ft)$. This equation accurately represents the motion of a horn during welding. In the clamping step simulation, the clamping pressure remained constant throughout the welding process. Table 4 lists the boundary conditions and loads of the components in both phases of ultrasonic welding.

Table 4. Boundary conditions and loads

Elements	Step 1		Step 2	
	Load	Displacement	Load	Displacement
Upper sheet		U_Y Free		U_X Free, U_Y Free
Lower sheet		U_Y Free		U_X Free, U_Y Free
Knurl	Pressure	U_Y Free	Pressure	$u(t) = u_0 sin(2\pi ft)$, U_Y Free
Anvil		Fixed		Fixed

3.5 Interactions

Two types of contacts were used in the 3D finite model. The first contact included two surface pairs: the top surface of the outermost sheet contacting the tip pair's lower surface and the sheet's lower surface contacting the higher surface of the anvil pair. The tool surface was designated the master surface to prevent unforeseen penetration. The workpieces were in contact via kinematic surface-to-surface contact. Heat conduction, represented by κ, between the components, was considered, with a conductance value of 235 W m^{-1} K^{-1}. Heat conduction facilitates the uninterrupted movement of heat from one component to another. A consistent friction coefficient was established using Eq. (14). In the current studies, all the unfixed edges, except for the contact surfaces shown in Figure 4, in the model are subjected to free convection. The convection coefficient is set at 30 W m^{-1} K^{-1}, and the ambient temperature is 24 °C.

3.6 Temperature Distribution in the Model

Figure 5 illustrates the thermal distribution observed during ultrasonic welding using a 20 µm amplitude, knurl vibration frequency of 20 kHz, and clamping pressure of 100 MPa at 0.01 s, 0.02 s, and 0.03 s. The temperature distribution was measured using a Celsius temperature scale. The temperature in the aluminum plates exhibited a rapid increase, with a rise of approximately 200 ºC occurring at approximately 0.01 seconds.

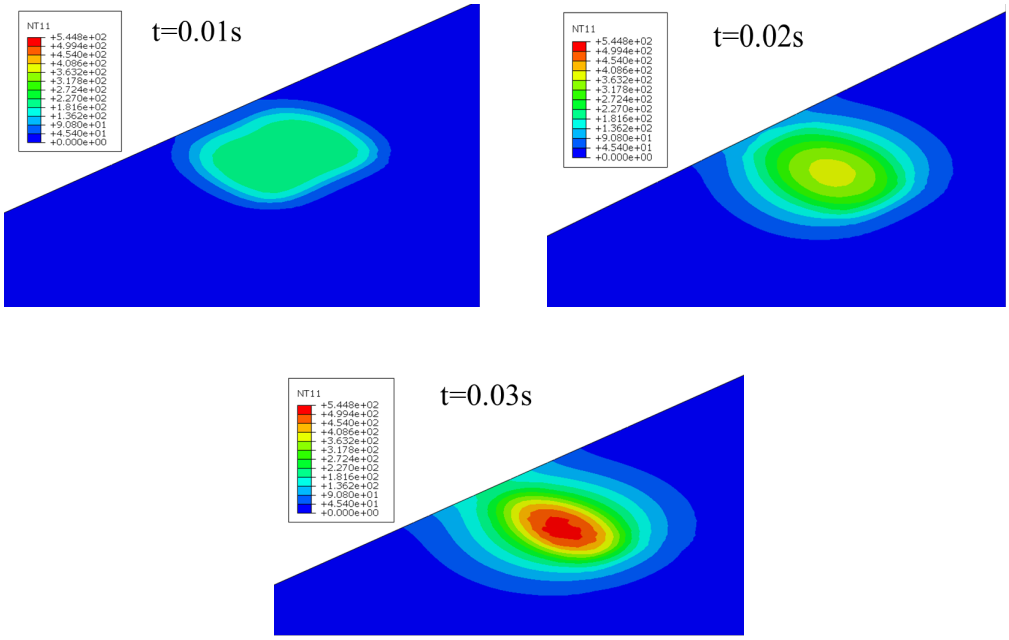

Figure 5. Temperature distribution at times of 0.01 s, 0.02 s and 0.03 s

These findings indicate that the duration of ultrasonic welding for materials with high heat conductivity, such as aluminium, is very short. Based on the simulation findings shown in Figure 5, it can be inferred that there is a direct correlation between the temperature increase and the duration of the welding operation. The modeling results are consistent with the experimental findings of Bakavos et al. [31], indicating that the temperature of the weld contact rapidly

reaches its peak value in under 1 second. Then, the temperature quickly declined due to the low input energy and good heat conductivity of the AA6061.

3.7 Stress Distribution in the Model

Ultrasonic welding subjects the base metal sheets to clamping force, high vibration frequency, and a temperature field that is not evenly distributed. Consequently, tension is generated at the welded connection. Figure 6 shows images of the simulations illustrating the von Mises stress and comparable plastic strains in the work materials during the UMW process. These images were taken after 0.03 seconds of welding. The tension reached its center at the knurl, resulting in the largest plastic deformation, as shown in Figure 6(a), and the maximum von Mises stress is 4.264×10^8 Nm^{-2}. The simulation findings indicate that the stress at the weld surface increases when the clamping force rises. Furthermore, the highest stress is observed within the centre of the sonotrode tip. This has also been tested by De Vries investigation [32]. Figure 6(b) shows that the plastic strain in the vibration direction was compressive, whereas the tensile strain was on the other side. This suggests that the knurl pattern exerted pressure on one side of the tab and relieved the pressure on the opposite side during each oscillation cycle. This was corroborated by the investigation conducted by Shen et al. [33], wherein they conducted simulations of the multi-layer metal ultrasonic welding process.

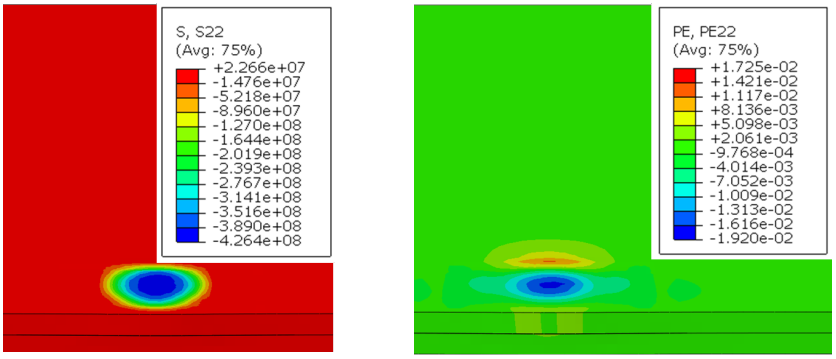

(a) von-Mises stress (b) Plastic strain

Figure 6. Contours for von Mises stress and plastic strain

Figure 7 illustrates the comparison of the deformation characteristics of the lower sheet with the plastic strain in the direction perpendicular to the plane after a welding period of 0.03 s. In direct contact with the vibrating horn, the upper tab had the most significant compressive plastic deformation, characterized by both tensile and compressive plastic strain of 1.92×10^{-2}, as shown in Figure 6(b). The plastic deformation progressively decreased in the bottom tab with the strain of 8.136×10^{-3}, as shown in Figure 7. This change rule is similar to the one employed in research [34]. The findings obtained from the clamping stage are shown in Figure 8. The displacement in the thickness direction exhibits viable values, considering the deformation value of -2.384×10^{-6} m at the center of the horn. Consequently, using ultrasonic vibration in the next step increased the temperature of the welded components. The pressure and vibration from the horn cause the temperature to rise, resulting in the expansion of the material. This expansion is directly proportional to temperature.

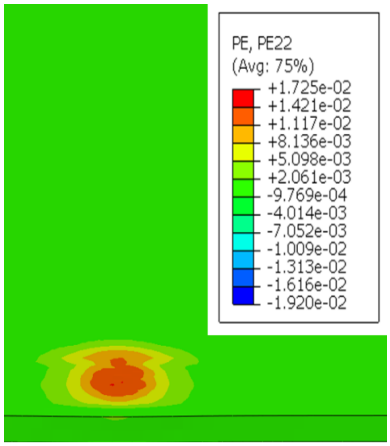

Figure 7. Plastic strain in the out-of-plane direction

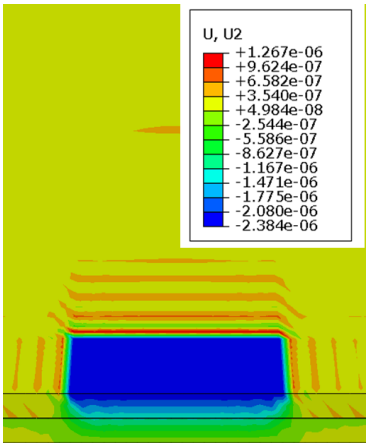

Figure 8. Displacement of the clamping step

3.8 Validation

This study conducted ultrasonic welding experiments using a frequency of 20 kHz, an amplitude of 20 µm, and a clamping pressure of 100 MPa, equivalent to a pressure of 5.5 bar applied to the ultrasonic welding machine. The experiment utilized ultrasonic welding equipment manufactured by UTHE Co. Ltd, a Japanese manufacturer, as shown in Figure 9(a). Figure 9(b) displays an infrared thermal imaging that records the temperature of the weld region after the horn has returned to its initial position. Figure 9(c) depicts the sample that has been welded successfully. The temperature measured in Figure 9(b) is an unreliable indication of the temperature during the ultrasonic welding operation. This is because the welding process is very short, and the infrared camera used to monitor the temperature is not fast enough to catch the temperature at the exact instant it occurs. So, this thermal imaging only illustrates the temperature concentration in the welding area during the ultrasonic welding process. The welded sample was successfully welded, as presented in Figure 9(c). The tensile strength of the welded conjunction was determined using experimental testing, which involved evaluating the outcomes of three welded samples. The mean achieved tensile strength was 84.7 MPa.

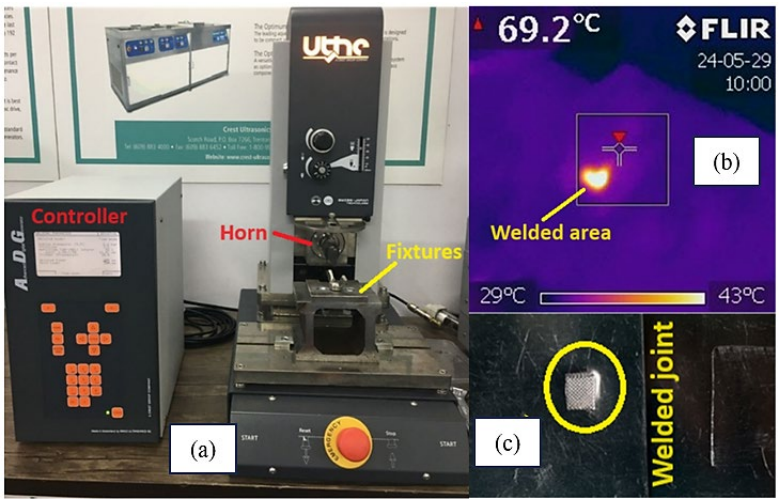

Figure 9. (a) Ultrasonic welding equipment, (b) Infrared thermal image, and (c) Welded joint

To verify our simulation model's precision, we directly compared the simulation results obtained in this work and the experimental findings done by Watanabe et al. [34]. The authors also investigated the application of ultrasonic welding on Al 6061 aluminium. The welding tip utilized in the experiment had dimensions of 10 mm x 10 mm, similar to those employed in our investigation. The frequency of oscillation used in [34] is 15 kHz. The temperature is measured at the periphery of the weld on the side of the specimen that is in contact with the anvil. To optimize computational efficiency, the simulation is limited to 0.03 seconds. The comparison results are presented in Figure 10.

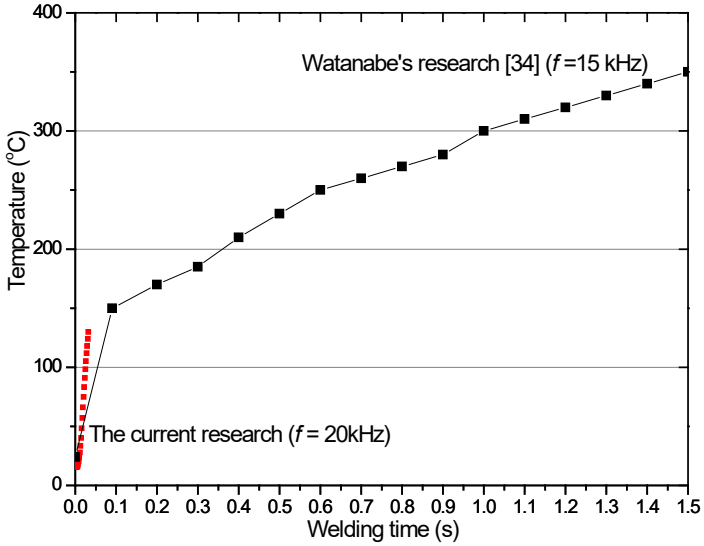

Figure 10. The comparison between the experiment [34] and the FEM temperature history

Watanabe conducted research in which the temperature was continuously monitored for 1.5 seconds. The comparison results strongly resemble the simulated results obtained in this work and the experimental data presented in reference

[34]. In the experiment conducted in reference [34], the rate of temperature change throughout the comparison time of 0.03 s was marginally lower than the values obtained from the simulation. The discrepancy can be attributed to the utilization of a lower oscillation frequency of 15 kHz in contrast to the simulation, which employed a frequency of 20 kHz. Hence, the findings unequivocally validated the precision of the simulation model employed in this study. Therefore, the finite element model employed in this work may be utilized to investigate the ultrasonic welding process further. This section details the welding zone as a basis for designing the ultrasonic welding process for aluminium materials. The parameters of the ultrasonic welding process used in these simulations were 20 kHz, 20 μm, and 100 MPa.

3.9 Temperature in the Welding Area

Figure 11 displays the temperature records at positions 1, 2, 3, and 4 on the upper plate in the region where the plate comes into contact with the horn. The temperature at position 3 reached a maximum value of 516 ºC. Despite being located near the central point of the horn, position 2 experienced a relatively modest temperature of approximately 426 ºC. This phenomenon may be due to the increased temperature in the welding area during the ultrasonic welding process, which causes the material to expand, exerting pressure on a specific part of the upper plate and ensuring continuous contact with the tip horn. Consequently, any movement between the horn tip and upper plate is minimal.

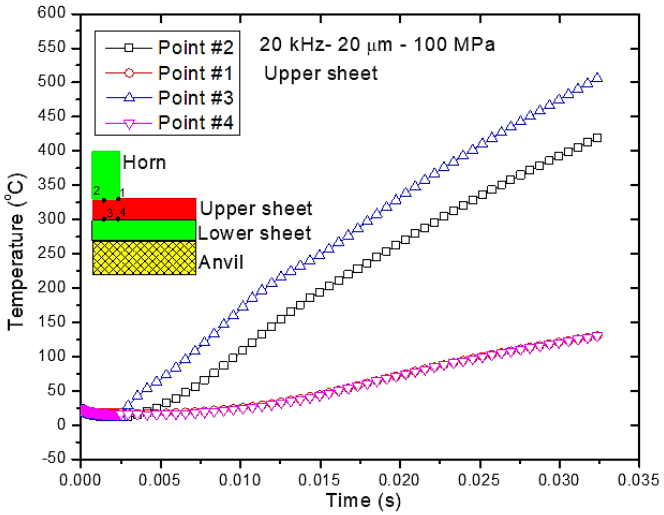

Figure 11. History of temperature variations at locations on the upper sheet

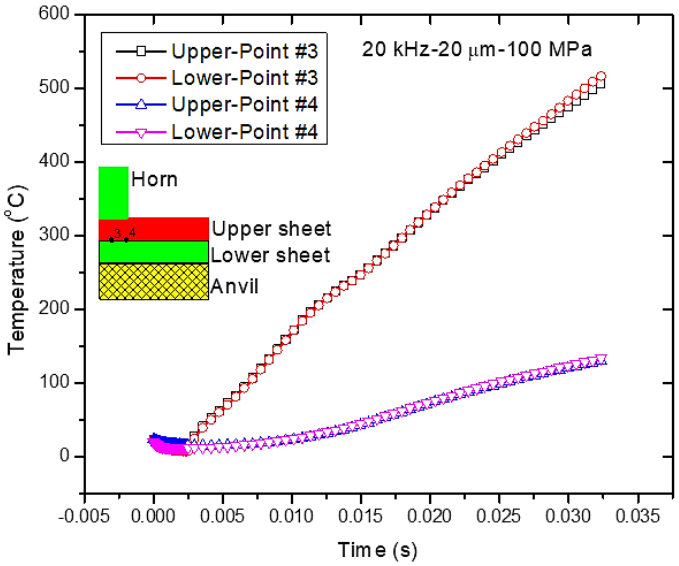

Figure 12. Upper and lower plate temperatures

The heat source detected at this location on the top plate is a passive heat source. The primary source of heat production occurred at position 3, which corresponded to the contact point between the two plates. The heat source diffused across the metal plates and transmitted thermal energy to locations 2, 4, and 1. It is evident that the temperatures at positions 1 and 4 exhibit a high degree of similarity, indicating that the heat at these sites is derived from heat transfer occurring at position 3. During the clamping phase, from the start to 2.5 ms, the temperature almost did not increase, but when starting

the ultrasonic welding phase, the temperature increased very quickly. The temperature at position 3 reached a weldable temperature of 500 ºC after 0.025 s. The temperature at position 3 increased quickly, whereas the temperature at position 4 increased insignificantly. Thus, the area of material that reaches the welding temperature for the connection is not the entire area in contact with the horn tip. Hence, the contact surface area between the horn and plate does not need to be large. Additional research also indicates that, on average, the temperature at the center of the weld interface is 50–130 °C greater than the temperature at the weld edge for different lengths, and the temperature difference between the weld interface and the top surface of aluminium sheet is about 58 ºC along the vertical direction of time during welding [35, 36]. Figure 12 shows the temperatures recorded at locations 3 and 4 on top and lower aluminium plates. The data shown in Figure 12 indicate that the temperatures at these locations were comparable. This may be explained by the fact that heat energy transfer remains constant when ultrasonic welding is performed on two similar materials.

3.10 Displacement of Upper Plate and Horn

Plastic deformation is necessary to guarantee the joining of the top plate and the horn. Figure 13 displays the predicted displacement of position 2 on both the top plate and the horn tip. The findings indicate that at position 2, the point of contact between the horn and the top plate and the displacements of both the horn and the upper plate are perfectly aligned. This demonstrates consistent and reliable contact between the horn tip and the surface of the metal plate. During the clamping period, under the impact of 100 MPa of pressure on the horn tip, the displacement at position 2 is -2 μm. When entering the ultrasonic welding stage, this displacement increased to -4 μm. However, the temperature increased rapidly during this stage, causing the material to expand, so the displacement increased in the opposite direction. This material expansion causes the upper plate to contact the horn tip. Elevated temperatures induce thermal expansion and softening of the material, thereby promoting the penetration of the horn into the upper plate, resulting in an enhanced connection between the horn and the upper plate.

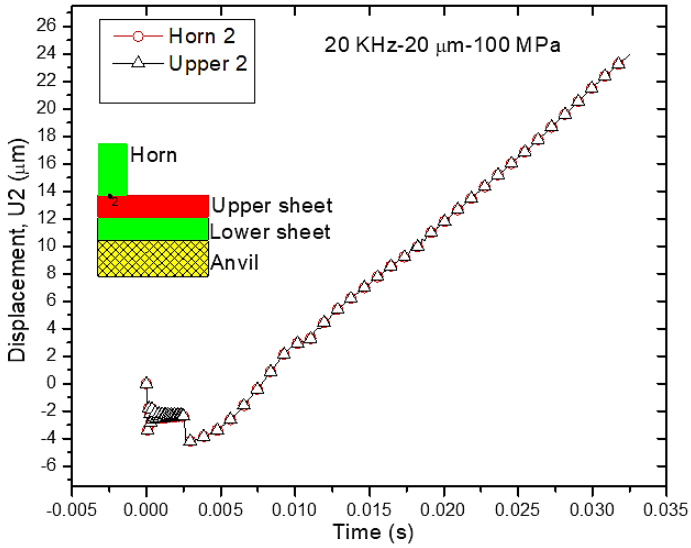

Figure 13. Displacement according to U_Y of the top plate and horn

Consequently, transferring vibrational energy to the top sample was more efficient. Therefore, there is an increased relative movement between the two plates because of the substantial vibrational energy transmitted from the tip of the horn. In contrast, when the temperature of the top plate exceeded the critical temperature, there was a gradual decrease in the bond strength between the upper plate and the horn tip. This is due to the softening of the material, which results in a reduction of the bond. Finally, the connection was not sufficiently strong to effectively transmit the excitation force from the horn. Consequently, the relative motion (sliding) between the horn and the upper plate progressively intensifies as the welding process approaches its final stage. Therefore, for the ultrasonic welding process to be efficient, providing a secure connection between the horn and the top plate is necessary. This allows for the most effective transmission of vibration energy from the horn to the aluminium plates. If there is a significant increase in the slippage of the horn towards the conclusion of the procedure, it indicates that the top layer has undergone excessive softening. The horn tip was occasionally textured with knurling to prevent potential slippage between the horn and the top plate. This simulation result aligns with the discoveries made by Shen et al. [33]. Shen's research shows apparent differences in the vertical movement of the horn when it vibrates at varying amplitudes. In the first stage, the curves depicting the motion of the horn tip with different amplitudes are nearly indistinguishable. Here, the different magnitudes of the amplitudes do not seem to impact the vertical movement of the horn. The curves start to deviate only when the horn reaches its maximum theoretical penetration depth, around 300 μm. The vertical displacement of the horn is maximized when the amplitude parameters are set to their maximum levels.

3.11 Displacement According to the U_X (Vibration) Direction of the Plates

The mobility of interfaces in the vibration direction is crucial for creating welds during ultrasonic welding. Increased relative motion may enhance the development of frictional heat and expedite the removal of surface impurities, thereby accelerating weld formation. Figure 14 depicts the displacement of the upper and lower plates at position 3 in the U_X direction, with amplitudes of 20 µm, 22 µm, and 25 µm, corresponding to a frequency of 25 kHz and a pressing pressure of 100 MPa. This direction allowed the aluminium plates to move unrestrictedly throughout the ultrasonic welding process. The two axes along which the components inside the aluminium panels have unrestricted movement are the U_Z- and U_Y-axes. The ultrasonic welding process may be categorized into three distinct stages [36]. During the first welding phase, the upper aluminium sheet experiences vibrations caused by the sonotrode point and slippage. In contrast, the bottom aluminium sheet stays stationary, resulting in a significant relative movement between the top and bottom sheets. During the second welding stage, the movement is limited due to the production of welded regions at the interface. Still, relative motion exists between the sonotrode tip and the top sheet. During the third step of welding, as the temperature of the welding interaction rises, both the top and bottom aluminium sheets undergo plastic deformation. The formation of welded regions occurs during the initial welding stage, expands during the subsequent welding stage, and the joint strength achieves its peak value in the final welding step. The third stage is a crucial phase in which the welded region experiences significant growth and expansion. This advancement is advantageous as it improves the resilience of the joint and transforms the connection between two surfaces into a central contact. Excessive welding energy leads to stage 4, causing a rapid drop in the velocity of both the top and bottom sheets. Simultaneously, sonotrode tip sticking (adhesion between the sonotrode tip and the top sheet) and weld zone thinning destroy the welded portions during stage 3, thus influencing the strength of the joint.

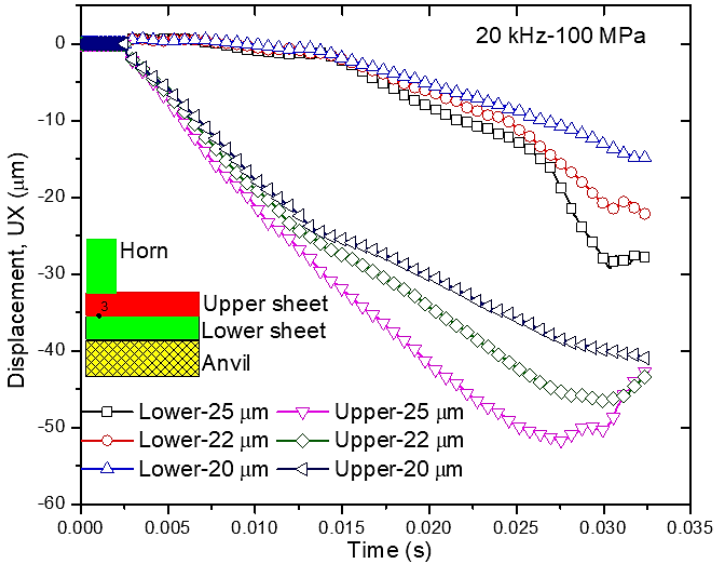

Figure 14. Displacement according to the U_X of the plate in amplitude

The rules governing the relative motion of the plates, as derived from our research, exhibit similarities to the previous states in [36]. As shown in Figure 14, during the clamping stage, the displacement of the aluminium plates remained constant, and there was no displacement. However, at the beginning of the welding process, the plates underwent a rapidly increasing displacement owing to the vibration of the horn tip. The top plate experienced a more rapid increase in displacement compared to the lower plate due to the direct reception of vibrations at the horn. The top plate experienced displacement at a higher velocity than the lower plate. Figure 14 shows a relative motion between the two aluminium plates at position 3. The lower plate does not move during a time of less than 0.015 s, while the upper plate moves according to the horn tip's vibration. This step represents the first stage of the ultrasonic welding process. Heat formation was caused by the sliding action between the two metal plates, resulting in friction. Hence, the heat generated during the ultrasonic welding procedure originated from position 3, the central contact point between the two plates. After 0.015 seconds, the bottom plate begins motion. Nevertheless, there remains a state of relative sliding between the two plates. This step is the second phase of the ultrasonic welding process, during which the formation of the weld happens. Phase 3 follows shortly after, as the temperature of the welding region rises.

The increased amplitude of oscillation leads to a corresponding increase in the movement speed of the plates, significantly affecting the movement of the upper plate, which receives energy directly from the horn tip. During the first phase of the ultrasonic welding process, the velocity of the motion of the plates did not exhibit a substantial disparity. However, the velocity exhibited a distinct change after a time interval of 0.015 s. As the welding process concluded, the plates' velocity increased. This phenomenon may be attributed to the inverse relationship between the temperature of the

plates and the friction coefficient. The friction coefficient decreased as the temperature increased, facilitating plate movement.

Figure 14 depicts the simulation results indicating that stage 4 of the ultrasonic welding process has occurred for oscillation amplitudes of 25 μm and 22 μm, accompanied by an oscillation frequency of 20 kHz. The displacement of the upper welded plate gradually decreases while that of the lower plate increases. As reference [36] stated, excessive heat reduces the weld joint's hardness. Consequently, this causes a decrease in the bond between the horn tip and the upper plate while increasing the bond between the horn tip and the lower plate. This is due to the thinning of the bond at the weld caused by overheating. This drop occurs after 0.025 s for 25 μm amplitude and after 0.03 s for 22 μm amplitude. An evaluation of the cycles in the ultrasonic welding process will assist in choosing appropriate welding parameters to avoid excessive heating. This discovery may be used to determine the optimal frequency, pressure, amplitude, and welding time for ultrasonic welding to prevent excessive heating that could reduce the tensile strength of the weld. This is advantageous since it eliminates the need to use expensive measuring equipment to determine the movement of the welded plates, hence reducing research costs.

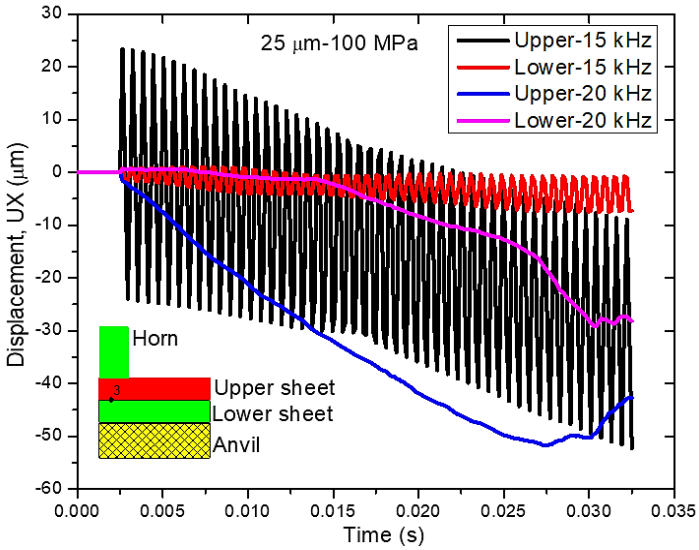

Figure 15. Stick-slip displacement of the plate when the oscillation frequency is low

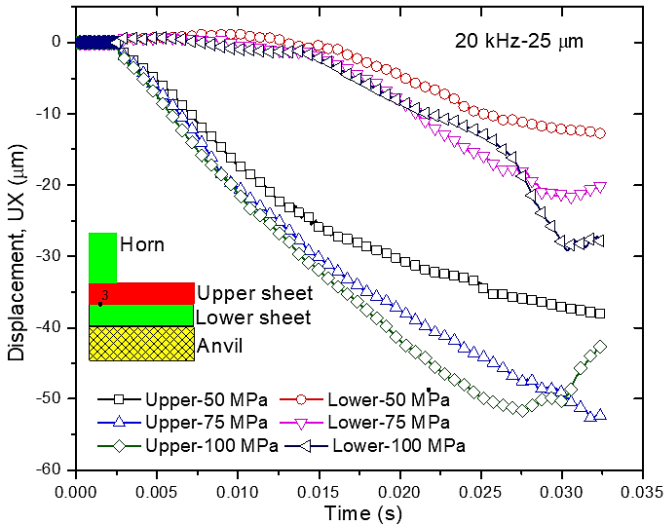

Figure 16. Displacement, according to U_X depends on pressure

The plates exhibited an unrestricted backward movement while the horn tip oscillated around its balance point. This occurs because the plates have greater inertia than the contact force from the horn tip, resulting in plates sliding in the direction of the least resistance. When the oscillation frequency of the horn head was high, the displacement of the upper and lower plates was in the same direction, and no oscillations appeared. In contrast, when the oscillation frequency of the horn tip was sufficiently low, the top plate exhibited a stick-slip motion, as shown in Figure 15. At a frequency of 15 kHz, the upper sheet exhibited stick-slip motion with an oscillation amplitude of approximately 40 μm, whereas the horn oscillated with an amplitude of 25 μm. Simultaneously, the lower plate vibrates in phase with the upper plate with an

amplitude of approximately 10 µm. Hence, it is advisable to ensure that the oscillation frequency of the horn in ultrasonic welding is sufficiently high to avoid the occurrence of stick-slip motion in aluminium plates, which might lead to oscillations in the clamping components during the welding process. The pressure also significantly affected the plates' displacement, causing relatively large movements between the plates and increasing the heat source. The results in Figure 16 show that with a small pressure, specifically 50 MPa, the displacement of the upper plate changes very little during the ultrasonic welding process. When the pressure increased to 75 and 100 MPa, the displacement of the plates increased correspondingly. The simulation findings depicted in Figure 16 indicate that stage 4 of the welding cycle occurred at pressures of 100 MPa and 75 MPa.

3.12 The Influence of Input Parameters of the Ultrasonic Welding Process

3.12.1 Influence of amplitude

The study indicated that even small fluctuations in horn vibration amplitude, typically within a range of a few micrometers, substantially influence the temperature and joint strength attained during the welding process. The temperature fluctuation at point 3 of the lower plate is shown in Figure 17. The oscillation amplitudes used were 20 µm and 25 µm, with an oscillation frequency of 25 kHz and pressure of 100 MPa. Despite the 5 µm amplitude difference, the temperatures achieved in these two situations vary dramatically. The rate of temperature escalation is greater at larger amplitudes than at smaller amplitudes. At the conclusion of the oscillation, the temperature reached a peak of approximately 700 ºC when the amplitude was 25 µm, which was much greater than the temperature of 500 ºC when the amplitude was 20 µm. As the temperature rises to approximately 700 °C, the material's yield strength diminishes, and softening of the material may be seen with changes in its microstructure, such as grain coarsening. The recrystallization temperature of aluminium varies between 425 and 650 °C, depending on the degree of deformation [31].

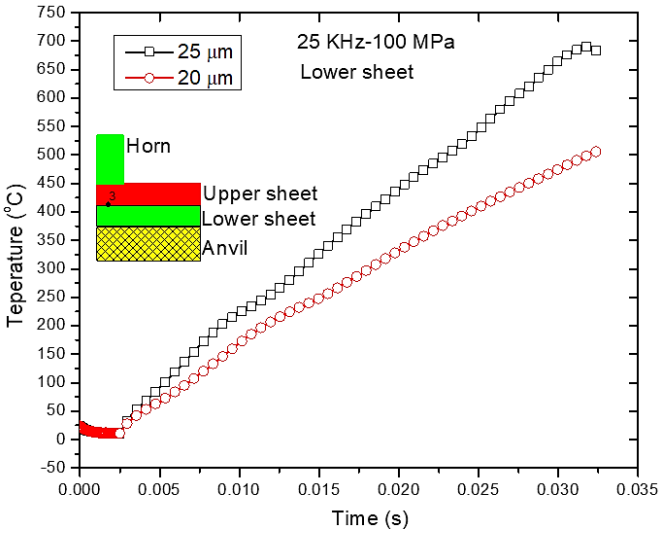

Figure 17. Effect of amplitude on temperature

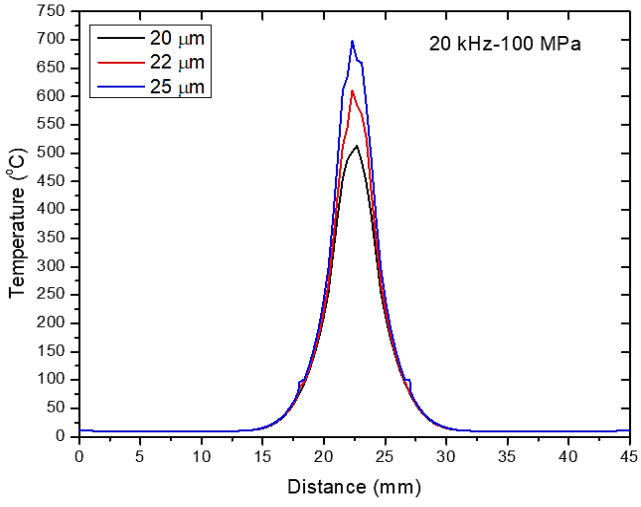

Figure 18. Effect of amplitude on heat affected zone width

At an amplitude of 25 µm, the temperature reached this range within approximately 0.025 s after the welding period began. As the stimulation amplitude increased, the overall motion throughout the entire friction system, including all contact surfaces, likewise increased. Consequently, welders with larger set amplitudes had more friction, resulting in a greater increase in temperature. Welds executed with large amplitudes exhibited the most rapid increase in temperature, particularly when the welding process reached its conclusion. Research conducted in [33] has also demonstrated that even little alterations in the magnitude of horn vibration, within a range of a few micrometers, substantially influence the temperatures and bonding strength attained during the welding process. The magnitude of vibration dictates the heat produced due to friction throughout the operation, determining the temperatures attained inside the welding region. Nevertheless, the magnitude of the amplitude had little impact on the width of the heat-affected region, as shown in Figure 18. Modifying the amplitude impacts the pace at which the heat rises and the maximum temperature while having little influence on the width of the heat-affected zone.

3.12.2 Effect of frequency

Figure 19 shows the simulation results of the lower plate's temperature change at point 3. The oscillation frequencies used were 15 kHz and 20 kHz. The oscillation amplitude was 25 µm, and the clamping force was 100 MPa. The findings indicate that when the oscillation frequency increases, the rate of temperature change increases proportionally. Specifically, when the frequency of oscillation increased, there was a notable increase in the size of the heat-affected zone, as shown in Figure 20. The size of the heat-affected zone expanded in direct proportion to the oscillation frequency. This phenomenon occurred because of the direct relationship between the increase in the oscillation frequency of the horn and the corresponding increase in the movement speed of the plates. Consequently, this leads to the expansion of the heat-affected region.

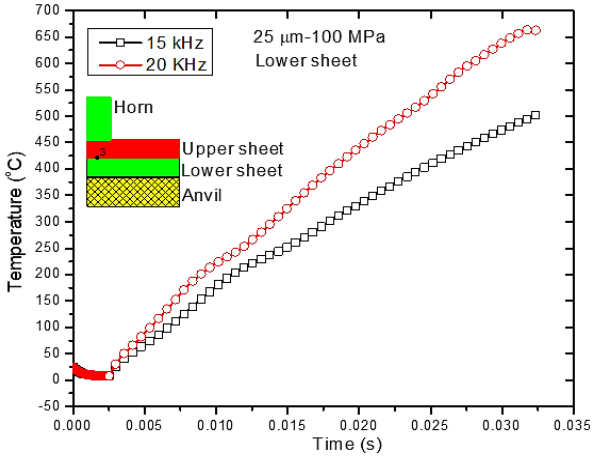

Figure 19. Effect of frequency on temperature

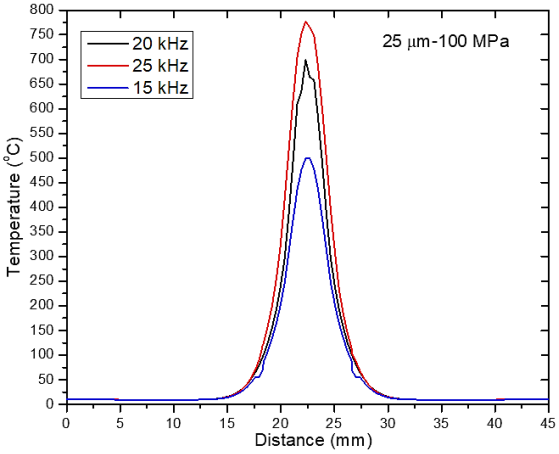

Figure 20. Effect of frequency on the width of the heat-affected zone

3.12.3 Effect of clamping pressure

The temperature gradient remained somewhat consistent as the clamping force increased from 75 to 100 MPa, as shown by the simulation results depicted in Figure 21. Therefore, augmenting the clamping force would not be favorable for the rapid ultrasonic welding procedure. Regarding the oscillation amplitude, the pushing force only enhances the temperature growth rate without affecting the width of the welding region, as shown in Figure 22. Hence, the pressure parameters, amplitude, and oscillation frequency significantly affect the temperature development during the ultrasonic welding process. An amplitude variation of only a few micrometers causes the temperature growth rate to fluctuate substantially. The pressure force has little influence on the input parameters of the ultrasonic welding process. The applied force must be of a sufficient magnitude to guarantee the transfer of the vibrational energy of the knurl to the plates. The oscillation frequency is a crucial input parameter significantly affecting the temperature increase rate and the welding zone's breadth. The primary reason for bond-to-bond deformation differences and the main contributor to unreliable bonds is the occurrence of low-frequency motion [2]. Designing an ultrasonic welding process with high oscillation frequency, appropriate oscillation amplitude, and minimal clamping force is advisable.

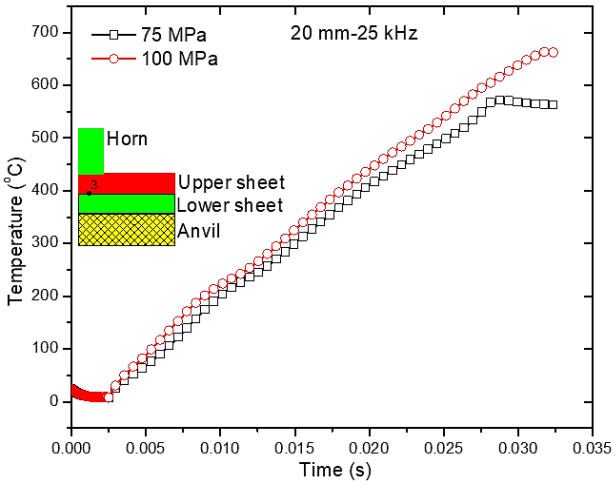

Figure 21. Temperature depends on the pressure

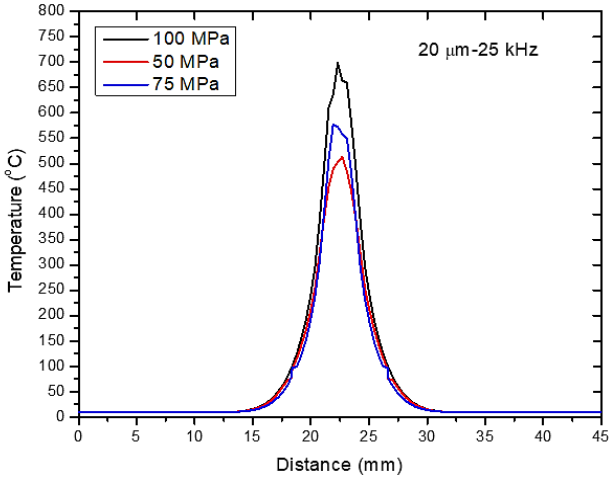

Figure 22. The width of the affected zone depends on the pressure

3.13 Ultrasonic Welding Process with Preheating

This section proposes a localized preheating method to improve the process stability and evaluates the influence of the preheating temperature on the welding process and performance using computational analysis. Localized preheating was conducted using the specialized equipment shown in Figure 23, focusing only on preheating the busbar. In practice, a type-K thermocouple is connected to a busbar located outside the welding area to monitor the temperature. The busbar is uniformly heated on the heating plate to a temperature 15–25 ºC higher than the intended preheating temperature.

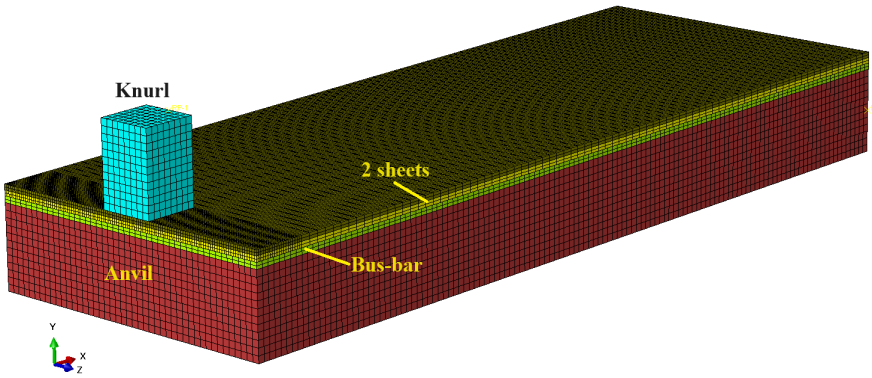

Figure 23. Geometry and mesh of the finite element model of preheating

Figures 24 and 25 show the simulated temperature distributions for the two preheating scenarios of 100 ºC and 150 ºC, respectively, and the surrounding environment at the conclusion of the 0.03-second welding duration. The highest temperature was consistently observed near the center of the weld and at the tabs in all instances. These findings align with prior simulations that used material characteristics comparable to the existing literature. The temperature distribution results between the two cases of heating the 100 ºC busbar plate and without heating were not significantly different, as shown in Figure 24. The highest temperature and width of the heat-affected zone in both cases were similar. However, a significant difference was observed when the preheating temperature was increased to 150 ºC, as shown in Figure 25. The results presented in Figure 25 show that the width of the heat-affected zone increased. In particular, the region with temperatures above 600 ºC is expanded significantly when ultrasonic welding was performed with preheating. Specifically, the diameter of the material area with a temperature above 600 ºC when preheating was 6 mm compared to that when ultrasonic welding without preheating was 5 mm. This indicated that the hardness of the preheated ultrasonic weld also increased. The findings indicate that preheating results in a more even temperature distribution throughout the workpiece and expands the heat-affected zone. The simulation findings achieved in this work assume that the welded plates possess a completely level surface. Evidence from experiments strongly shows that the surface of these panels is uneven. The heat generated during the ultrasonic welding process is heavily influenced by the contact parameters of the two surfaces of the welded pieces. Hence, a comprehensive investigation of ultrasonic welding that considers the surface roughness of the plates is quite beneficial.

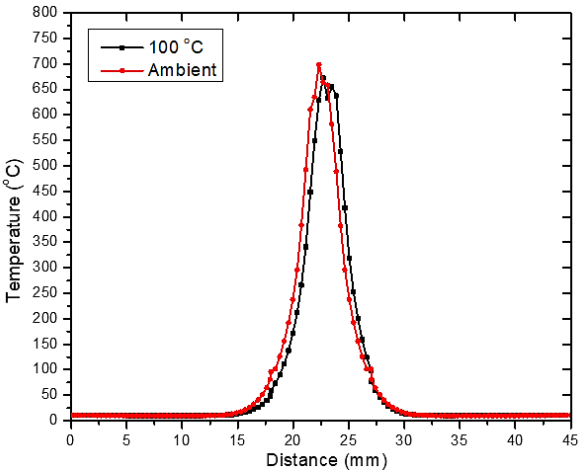

Figure 24. Width of heat affected zone of 100 ºC preheating

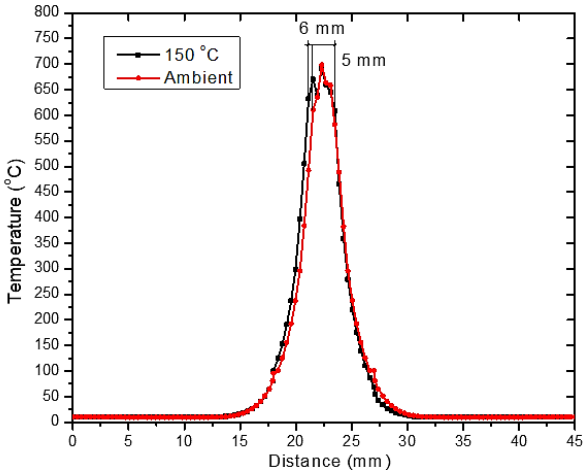

Figure 25. Width of heat affected zone of 150 ºC preheating

3.14 Analysis of Mesh Sensitivity

The mesh size significantly impacts the accuracy of predictions, especially when the numerical model involves plastic deformation. In the case of ultrasonic welding, the weld piece located close to the tip of the sonotrode experiences a notable concentration of stress, leading to a substantial indentation as the temperature rises. In this study, we examine the impact of mesh size. The model only simulated a 0.01 s episode since the whole welding process is computationally expensive. We investigated five models with varying minimum mesh sizes ranging from 200 µm to 600 µm. Within this set of models, the sonotrode meshes remain consistent as the tool material exhibits purely elastic behavior. The study analyzed five models with varying minimum mesh sizes ranging from 200 to 600 µm. The details may be seen in Table 5.

Table 5. The computational expense associated with a 0.1 s

Model No.	1	2	3	4	5
Min. element size (µm)	600	500	400	300	200
Stable time increment (s)	4.437×10^{-8}	4.024×10^{-8}	3.048×10^{-8}	2.703×10^{-8}	1.985×10^{-8}
Number of increments	225,371	248,507	288,289	369,938	503,865
Computation time (s)	15,060	19,620	52,680	68,340	139,860

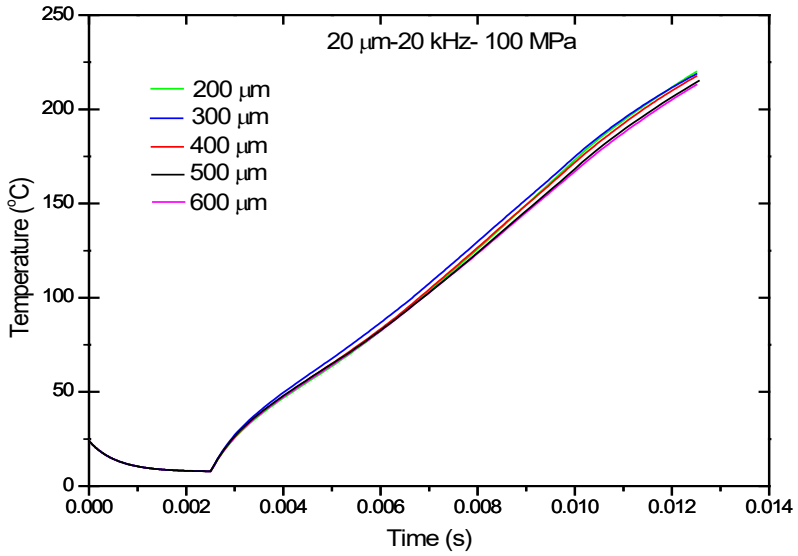

Figure 26. Instantaneous temperature at the midpoint of the faying contact

The results depicted in Figure 26 indicate that Model-1 and Model-2, which employ a mesh size greater than 400 µm, provide temperature profiles that significantly deviate from those produced using lower meshes. The results of Model-3, with a parameter value of 400 µm, display several inconsistencies in the initial stage. Nevertheless, the forecasts generally

correspond to those of Model 4 and Model 5. According to the temperature data obtained from the simulations, a minimum mesh size of 400 μm is required to effectively investigate thermomechanical behaviour variations during all USW process phases.

4. CONCLUSIONS

The 3D numerical simulation approach proposed in this study is currently the most effective and all-encompassing option for modelling intricate materials in the UMW process while offering scientific comprehension and technical instruction. The outcomes of shortened USW simulations, conducted with a restricted welding duration, indicate that:

i) A detailed 3D thermal-mechanical model has been developed for the ultrasonic welding process of Al 6061. This model considers heat generation in gaps, acoustic softening, a mesh size smaller than 400 μm, and a variable friction coefficient.

ii) The numerical model was verified using the temperature contour from a reference study.

iii) The pressure parameters, amplitude, and oscillation frequency in ultrasonic welding significantly influence the temperature increase throughout the operation. A small change in amplitude, of only a few micrometers, can lead to significant fluctuations in the rate of temperature increase. The pressure minimally affects the input parameters of the ultrasonic welding process. The force exerted must be chosen at a level that ensures the transmission of the vibrational energy of the knurl to the plates. The oscillation frequency is a critical input parameter that has a considerable impact on both the pace of temperature increase and the width of the welding zone.

iv) Ultrasonic welding with preheating resulted in a much larger heat-affected area than ultrasonic welding without heating. The preheating temperature for ultrasonic welding of aluminum should exceed 150 ºC. A certain threshold of joining temperatures and plastic deformation is necessary to achieve a good level of joint quality. Conversely, high temperatures or plastic deformation might diminish the strength once again.

v) The simulation model predicts the displacement of the welded plates to determine the optimal frequency, pressure, amplitude, and welding time for ultrasonic welding to avoid excessive heating, which can reduce the tensile strength of the welded joint. This is advantageous since the approach eliminates the need for costly measurement equipment to detect the welded plates' motion, reducing research expenses.

vi) To prevent stick-slip motions of the welding plates during the ultrasonic welding process, the oscillation frequency of the horn tip must be more than 15 kHz.

In the future, 3D modelling can expedite the advancement of welding processes and reduce resources by conducting simulations that explore different process parameters within certain limits. Correlations can be established between the quality of the weld and models that incorporate the material's dynamic behavior, temperature distribution, or thermal history. Research on the impact of surface roughness on the thermal generating process in ultrasonic welding might be of interest.

ACKNOWLEDGEMENTS

Ho Chi Minh City University of Industry and Trade, Vietnam, sponsored and funded this research under Contract No. 76/HD-DCT, dated August 15, 2023.

CONFLICT OF INTEREST

The authors declare no conflicts of interest. There are no conflicts of interest with the submission of this manuscript, and all the writers have agreed that it can be published. This paper has not been published before, is not currently being reviewed by any other journal, and will not be sent anywhere else until this journal decides.

AUTHORS CONTRIBUTION

Le T. Truyen (Conceptualization; Methodology; Software; Data curation; Validation; Formal analysis; Writing - original draft; Writing - review and editing; Visualization)

Ho T. M. Nu (Validation; Conceptualization; Methodology; Writing–original draft; Writing–review and editing)

Dinh L. C. Ky (Methodology; Writing - original draft)

AVAILABILITY OF DATA AND MATERIALS

The data supporting this study’s findings are available on request from the corresponding author.

ETHICS STATEMENT

Not applicable

REFERENCES

[1] P. Bansal, K. M. Kockelman, "Forecasting Americans' long-term adoption of connected and autonomous vehicle technologies," *Transportation Research Part A: Policy and Practice*, vol. 95, pp. 49-63, 2017.

[2] G. Harman, J. Albers, "The ultrasonic welding mechanism as applied to aluminum-and gold-wire bonding in microelectronics," IEEE *Transactions on parts, hybrids, and packaging*, vol. 13, no. 4, pp. 406-412, 1977.

[3] J. Tsujino, K. Hidai, A. Hasegawa, R. Kanai, H. Matsuura, K. Matsushima, et al., "Ultrasonic butt welding of aluminum, aluminum alloy, and stainless-steel plate specimens," *Ultrasonics*, vol. 40, no. 1-8, pp. 371-374, 2002.

[4] T. Watanabe, H. Sakuyama, A. Yanagisawa, "Ultrasonic welding between mild steel sheet and Al–Mg alloy sheet," *Journal of* Materials *Processing Technology*, vol. 209, no. 15-16, pp. 5475-5480, 2009.

[5] C. Kong, R. Soar, P. Dickens, "Characterisation of aluminium alloy 6061 for the ultrasonic consolidation process," *Materials Science and Engineering: A*, vol. 363, no. 1-2, pp. 99-106, 2003.

[6] C.-Y. Kong, R. C. Soar, P. M. Dickens, "A model for weld strength in ultrasonically consolidated components," *Proceedings of the Institution of Mechanical Engineers, Part C: Journal of Mechanical Engineering Science*, vol. 219, no. 1, pp. 83-91, 2005.

[7] C. Kong, R. Soar, P. Dickens, "Optimum process parameters for ultrasonic consolidation of 3003 aluminium," *Journal of Materials Processing Technology*, vol. 146, no. 2, pp. 181-187, 2004.

[8] M. de Leon, H.-S. Shin, "Weldability assessment of Mg alloy (AZ31B) sheets by an ultrasonic spot-welding method," *Journal of* Materials *Processing Technology*, vol. 243, pp. 1-8, 2017.

[9] Z. Yang, Z. Wang, "Cyclic deformation and fracture behavior of Al alloy 6061 under the action of positive mean stresses," *Metallurgical Transactions A*, vol. 24, pp. 2083-2093, 1993.

[10] X. Cheng, X. Li, "Investigation of heat generation in ultrasonic metal welding using micro sensor arrays," *Journal of Micromechanics and Microengineering*, vol. 17, no. 2, p. 273, 2007.

[11] I. Balz, E. Abi Raad, E. Rosenthal, R. Lohoff, A. Schiebahn, U. Reisgen, et al., "Process monitoring of ultrasonic metal welding of battery tabs using external sensor data," *Journal of Advanced Joining Processes*, vol. 1, p. 100005, 2020.

[12] J. Zhao, H. Li, H. Choi, W. Cai, J. A. Abell, X. Li, "Insertable thin film thermocouples for in situ transient temperature monitoring in ultrasonic metal welding of battery tabs," *Journal of Manufacturing Processes*, vol. 15, no. 1, pp. 136-140, 2013.

[13] S. Elangovan, S. Semeer, K. Prakasan, "Temperature and stress distribution in ultrasonic metal welding—An FEA-based study," *Journal of Materials Processing Technology*, vol. 209, no. 3, pp. 1143-1150, 2009.

[14] A. Siddiq, E. Ghassemieh, "Theoretical and FE analysis of ultrasonic welding of aluminum alloy 3003," *Journal of Manufacturing Science and Engineering*, vol. 131, no. 4, p. 041007, 2009.

[15] P. Jedrasiak, H. Shercliff, Y. Chen, L. Wang, P. Prangnell, J. Robson, "Modeling of the thermal field in dissimilar alloy ultrasonic welding," *Journal of Materials Engineering and Performance*, vol. 24, pp. 799-807, 2015.

[16] D. Lee, E. Kannatey-Asibu, W. Cai, "Ultrasonic welding simulations for multiple layers of lithium-ion battery tabs," *Journal of Manufacturing Science and Engineering*, vol. 135, no. 6, p. 061011, 2013.

[17] K. Chen, Y. Zhang, "Numerical analysis of temperature distribution during ultrasonic welding process for dissimilar automotive alloys," *Science and Technology of Welding and Joining*, vol. 20, no. 6, pp. 522-531, 2015.

[18] H. Li, B. Cao, J. Liu, J. Yang, "Modeling of high-power ultrasonic welding of Cu/Al joint," *The International Journal of Advanced* Manufacturing *Technology*, vol. 97, pp. 833-844, 2018.

[19] J.-L. Chaboche, "A review of some plasticity and viscoplasticity constitutive theories," *International Journal of plasticity*, vol. 24, no. 10, pp. 1642-1693, 2008.

[20] B. K. Chun, H. Y. Kim, J. K. Lee, "Modeling the Bauschinger effect for sheet metals, part II: Applications," *International Journal of Plasticity*, vol. 18, no. 5-6, pp. 597-616, 2002.

[21] J. L. Chaboche, "Viscoplastic constitutive equations for the description of cyclic and anisotropic behaviour of metals," *Bulletin de I'Academie Polonaise des Sciences Serie des Sciences Technique*, vol. 25, no. 1, pp. 39-48, 1977.

[22] N. Ohno, J.-D. Wang, "Kinematic hardening rules with critical state of dynamic recovery, part I: Formulation and basic features for ratchetting behavior," *International Journal of Plasticity*, vol. 9, no. 3, pp. 375-390, 1993.

[23] T. Srivatsan, S. Sriram, C. Daniels, "Influence of temperature on cyclic stress response and fracture behavior of aluminum alloy 6061," *Engineering Fracture Mechanics*, vol. 56, no. 4, pp. 531-550, 1997.

[24] G. R. Johnson, W. H. Cook, "Fracture characteristics of three metals subjected to various strains, strain rates, temperatures and pressures," *Engineering Fracture Mechanics*, vol. 21, no. 1, pp. 31-48, 1985.

[25] J. G. Kaufman. Properties of Aluminum Alloys: Tensile, Creep, and Fatigue Data at High and Low Temperatures, 1st Ed. United States: ASM international, 1999.

[26] B. Langenecker, "Effects of ultrasound on deformation characteristics of metals," *IEEE Transactions on Sonics and Ultrasonics*, vol. 13, no. 1, pp. 1-8, 1966.

[27] S. Song, M. Yovanovich, F. Goodman, "Thermal gap conductance of conforming surfaces in contact," *Journal of Heat Transfer*, vol. 115, pp. 533-540, 1993.

[28] K. Chen, Y. Zhang, "Mechanical analysis of ultrasonic welding considering knurl pattern of sonotrode tip," *Materials & Design*, vol. 87, pp. 393-404, 2015.

[29] C. Zhang, X. Zhu, L. Li, "A study of friction behavior in ultrasonic welding (consolidation) of aluminum," in *Proceedings of the* AWS *Conference: Session 7: Friction and Resistance Welding/Materials Bonding Processes*, pp. 151-157, 2006.

[30] N. R. Naidu, S. G. S. Raman, "Effect of contact pressure on fretting fatigue behaviour of Al–Mg–Si alloy AA6061," *International Journal of Fatigue*, vol. 27, no. 3, pp. 283-291, 2005.

[31] D. Bakavos, P. Prangnell, "Mechanisms of joint and microstructure formation in high power ultrasonic spot welding 6111 aluminium automotive sheet," *Materials Science and Engineering: A*, vol. 527, no. 23, pp. 6320-6334, 2010.

[32] E. de Vries, "Mechanics and mechanisms of ultrasonic metal welding," *Ph.D. Thesis*, The Ohio State University, United States, 2004.

[33] N. Shen, A. Samanta, W. W. Cai, T. Rinker, B. Carlson, H. Ding, "3D finite element model of dynamic material behaviors for multilayer ultrasonic metal welding," *Journal of Manufacturing Processes*, vol. 62, pp. 302-312, 2021.

[34] T. Watanabe, H. Itoh, A. Yanagisawa, M. Hiraishi, "Ultrasonic welding of heat-treatable aluminium alloy A6061 sheet," *Welding International*, vol. 23, no. 9, pp. 633-639, 2009.

[35] E. Sooriyamoorthy, S. P. John Henry, P. Kalakkath, "Experimental studies on optimization of process parameters and finite element analysis of temperature and stress distribution on joining of Al–Al and Al–Al_2O_3 using ultrasonic welding," *The International Journal of Advanced Manufacturing Technology*, vol. 55, no. 5, pp. 631-640, 2011.

[36] C. Zhang, H. Li, Q. Liu, C. Huang, K. Zhou, "Ultrasonic welding of aluminum to steel: A review," *Metals*, vol. 13, no. 1, p. 29, 2023.